NANO · MICRO small
www.small-journal.com

Nonlinear All-Optical Coherent Generation and Read-Out of Valleys in Atomically Thin Semiconductors

*Paul Herrmann, Sebastian Klimmer, Thomas Lettau, Mohammad Monfared, Isabelle Staude, Ioannis Paradisanos, Ulf Peschel, and Giancarlo Soavi**

With conventional electronics reaching performance and size boundaries, all-optical processes have emerged as ideal building blocks for high speed and low power consumption devices. A promising approach in this direction is provided by valleytronics in atomically thin semiconductors, where light-matter interaction allows to write, store, and read binary information into the two energetically degenerate but non-equivalent valleys. Here, nonlinear valleytronics in monolayer WSe_2 is investigated and show that an individual ultrashort pulse with a photon energy tuned to half of the optical band-gap can be used to simultaneously excite (by coherent optical Stark shift) and detect (by a rotation in the polarization of the emitted second harmonic) the valley population.

1. Introduction

While conventional electronics is reaching performance limits in terms of speed and size[1], societal needs call for novel methods to provide greener, faster, and smaller gates to write, read, and store information. Light is the ideal candidate to realize devices operating with high speed and low power consumption thanks to all-optical operations[2,3] and lightwave electronics,[4–6] which promise to reach ≈THz bandwidths. In parallel, the frontiers of miniaturization in photonics and optoelectronics are nowadays accessible thanks to atomically thin materials[7] and hybrid structures.[8] To this end, nonlinear optics[9] in graphene and related materials[10] has already provided evidence of high-speed and broadband modulation of light[2,3,11] as well as ultrafast gates for optoelectronic logic operations.[12–14] Another promising approach to exploit the optical properties of 2D materials, and in particular of transition metal dichalcogenides (TMDs), is based on valleytronics.[15] TMD monolayers are direct bandgap semiconductors[16] and possess two energetically degenerate but non-equivalent valleys at the K and K' points of the Brillouin zone (**Figure 1**a). The valleys can be selectively excited by circularly polarized light of opposite helicity, generating a carrier population imbalance linked to the valley polarization (VP)[17–19] (Figure 1b). Thus, the VP represents a powerful tool for optoelectronic[20,21] and all-optical information processing at the nanoscale.

The optical generation (write) of the VP in TMDs has been achieved so far with different methods, including one-photon CW excitation,[17,18] nonlinear two-photon absorption (TPA)[22] and coherent excitation by optical Stark and Bloch–Siegert Floquet states.[23,24] The first two methods respond to different selection rules due to the conservation of angular momentum:[25] while one-photon excitation can reach the 1*s*, 2*s*, etc. states of the exciton Rydberg series, two-photon excitation is only possible into the 2*p* excited state[26] (Figure 1b), which in TMDs is typically >0.1 eV above the lowest 1*s* energy level.[27–29] With one-photon excitation, a VP of 100 % was observed in MoS_2 excited at 633 nm and at a temperature of 14 K to match the absorption line of the A exciton.[17] Two-photon resonant excitation on the 2*p* state in WSe_2, instead showed a maximum VP of 45% at a temperature of 4 K.[22] However, the VP decreases drastically when the lattice temperature increases, mainly due to the presence and impact of phonon-assisted intervalley scattering[18] and long-range electron-hole exchange interactions.[30] Indeed, the

P. Herrmann, S. Klimmer, I. Staude, G. Soavi
Institute of Solid State Physics
Friedrich Schiller University Jena
Helmholtzweg 5, 07743 Jena, Germany
E-mail: giancarlo.soavi@uni-jena.de
S. Klimmer
ARC Centre of Excellence for Transformative Meta-Optical Systems, Department of Electronic Materials Engineering, Research School of Physics
The Australian National University
Canberra ACT 2601, Australia
T. Lettau, M. Monfared, U. Peschel
Institute of Condensed Matter Theory and Optics
Friedrich Schiller University Jena
Max-Wien-Platz 1, 07743 Jena, Germany
I. Staude, U. Peschel
Abbe Center of Photonics
Friedrich Schiller University Jena
Albert-Einstein-Straße 6, 07745 Jena, Germany
I. Staude
Institute of Applied Physics
Friedrich Schiller University Jena
Albert-Einstein-Straße 15, 07745 Jena, Germany
I. Paradisanos
Institute of Electronic Structure and Laser
Foundation for Research and Technology
N. Plastira 100, Vassilika Vouton, 70013 Heraklion, Crete, Greece

The ORCID identification number(s) for the author(s) of this article can be found under https://doi.org/10.1002/smll.202301126

DOI: 10.1002/smll.202301126

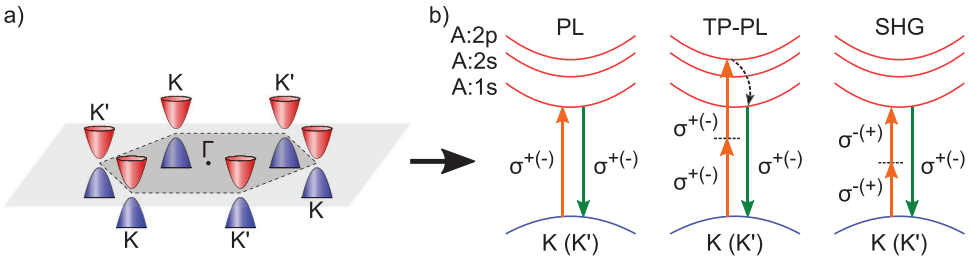

Figure 1. Valley selection rules in TMD monolayers a) First Brillouin zone with the energy-degenerate but non-equivalent *K*/*K*′ valleys. b) Selection rules for one-photon PL, TP-PL, and SHG in the excitonic quasi-particle picture. PL: photoluminescence; TP-PL: two-photon photoluminescence; SHG: second harmonic generation.

highest reported value of VP at room temperature in WSe_2 was only 16 %.[31] Although TPA leads to a lower degree of VP compared to one-photon excitation, it is experimentally more convenient as it allows to easily separate and filter the excitation and detection wavelengths. Finally, coherent VP excitation by optical Stark effect or Bloch–Siegert Floquet states does not involve the generation of a real excited state population, but rather an asymmetric and valley selective energy shift.[23,24] The main advantage of this approach is the ultrafast VP switching speed, which is inherently provided by the coherent nature of these processes.

The detection (read) of the VP was so far mostly based on polarization-resolved photoluminescence (PL): the (one-photon) spontaneous emission from the two non-equivalent valleys follows the same selection rules of the (one-photon) excitation/absorption.[17,18,32,33] However, this approach has two main drawbacks. First, it detects an averaged light emission over a time scale that is much longer compared to the valley and spin lifetimes,[34] and thus can not provide a precise estimate of the time-dependent (ultrafast) VP state. Second, it is intrinsically a destructive method, which measures the VP only after recombination of the electron-hole pair. Recently, second harmonic generation (SHG) has been proposed as an alternative approach to measure the VP in TMDs:[35–37] selective excitation of one valley breaks time-reversal symmetry and thereby reduces the intrinsic D_{3h} symmetry, leading to new terms in the nonlinear optical susceptibility of the TMD.[35] Compared to the measurement of the VP *via* PL, this approach has the distinct advantages of being ultrafast and non destructive, thus providing a more efficient building block for valleytronic devices. To date, experimental measurements of the VP by SHG are limited to references.[38,39] In both experiments, an elliptically polarized pulse is used to simultaneously generate and read the valley imbalance. However, Ho *et al.*[38] use a quasi-resonant excitation at 780 nm in $MoSe_2$. This corresponds to one photon absorption in a high excitation density regime (*i.e.*, close to the Mott transition) due to the strong pump laser needed to observe SHG. In addition, the emitted SHG probes a region (in the UV) far from the optical gap, thus likely less sensitive to the VP. Mouchliadis *et al.*[39] use a wavelength of 1030 nm in WSe_2 and WS_2. They observe an enhancement of the valley SHG term for decreasing temperatures in the range of 300 to 78 K. This was assigned to a more stable VP and longer valley lifetime at cryogenic temperatures compared to room temperature. Indeed, the low value of VP reported for any TMD at room temperature [31,33,40] further clarifies one of the main advantages of valley SHG, which allows to probe the VP on ultrafast time-scales, thus before the detrimental effect of exciton-phonon scattering. However, the authors in Ref.[39] did not discuss how the VP was generated, considering that the fundamental excitation is well below the optical gap and thus one-photon excitation is highly unlikely. In addition, the SHG at 515 nm is much higher than the optical gap, thus not ideal to probe the VP.

In this work, we simultaneously pump (write) and probe (read) the VP in WSe_2 with one single elliptically polarized ultra-short (≈150 fs) pulse at room temperature (see **Figure 2**). We study the VP at different values of the fundamental wavelength (FW) corresponding to below-gap (1600 nm), 1*s* resonant (1500 nm), and 2*p* resonant (1360 nm) SHG in WSe_2. We observe the largest VP for excitation at 1500 nm, where we measure a $|\chi^{(2)}_{VP}/\chi^{(2)}_{I}|$ of 18.8 % (with $\chi^{(2)}_{VP}$ and $\chi^{(2)}_{I}$ being the valley and intrinsic nonlinear optical susceptibilities, respectively, see Sections S3 and S4, Supporting Information), which is one order of magnitude larger compared to the values of 1.9% and 1.8% obtained at 1600 and 1360 nm. While this result looks obvious if we consider only the detection (read) of the VP, which is enhanced for resonant SHG at the 1*s* state, it provides additional useful information when we consider the excitation mechanism (write) of the VP. Looking at the combined results of two-photon photoluminescence (TP-PL) measurements and power-dependent valley SHG, we deduce that the VP observed in our experiments is generated by ultrafast coherent optical Stark shift. Furthermore, we show that our experimental results are well reproduced by theoretical simulations and modeling based on the semiconductor Bloch equations (SBE) and time-dependent density functional theory (TDDFT). This work provides direct evidence of ultrafast and all-optical coherent generation and detection of valleys in atomically thin semiconductors.

2. Results and Discussion

For the experiments, a WSe_2 monolayer is prepared and characterized as described in Experimental Section. Valley SHG measurements were performed using a home-built multi-photon microscope setup (Figure 2c). Achromatic half (HWP) and quarter-wave plates (QWP) allow for individual control of the tilt θ and ellipticity ϵ angles of the FW. Details on how to extract the degree of VP from the SHG intensity are reported in ref.[38] and in Section S4 (Supporting Information).

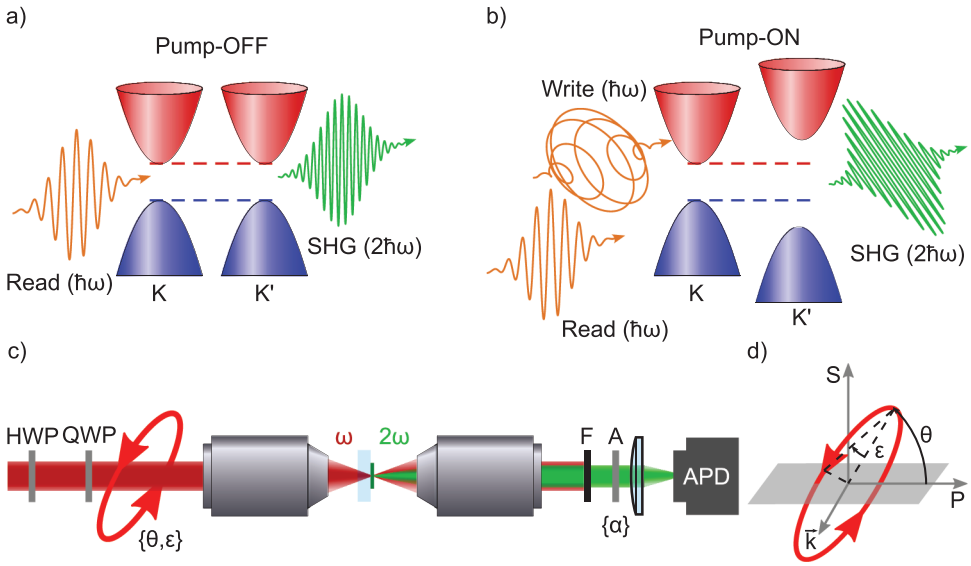

Figure 2. Write and read mechanism of VP and experimental setup. a) Without a circularly polarized write pulse (pump-OFF) the polarization of the SH signal generated by the read pulse is determined solely by crystal symmetry. b) VP is generated by the optical Stark effect induced by a circularly polarized write pulse (pump-ON), resulting in a rotation of the emitted SHG with respect to the pump-OFF case. c) Sketch of the experimental setup. HWP: half-wave plate; QWP: quarter-wave plate; F: filter; A: analyzer; APD: avalanche photodiode. d) Definition of the polarization ellipse parameters, the tilt (θ) is defined as the angle between the major axis of the ellipse and the axis of P-polarization (*i.e.* laboratory x-axis) and the ellipticity angle (ϵ) is the angle between the semi-minor and semi-major axis of the ellipse.

2.1. Characterization of SHG and TP-PL in Monolayer WSe_2

We first characterize the wavelength dependence of the TP-PL and SHG in our WSe_2 monolayer sample using a spectrometer (**Figure 3**a). When considering Gaussian beams, the relation between the full width at half maximum (FWHM) of the FW with respect to the SH signal scales as $\Delta\lambda_{SH} = \frac{1}{2\sqrt{2}}\Delta\lambda_{FW}$,[41] see Section S1 (Supporting Information) for details. Our source has a FWHM of ≈25 nm at a central wavelength of 1500 nm, and we observe a FWHM at the SH of ≈8 nm, in agreement with the aforementioned estimate. The integrated TP-PL (red dots) and SHG (black dots) for the different FW used in our experiments are shown in Figure 3b. The TP-PL is maximum when the FW is ≈1360 nm, in correspondence of the A exciton 2*p* state, as already reported by previous studies on WSe_2.[22] The maximum of the TPA efficiency on the 2*p* state is a direct consequence of optical selection rules on the exciton Rydberg series. For the same FW, also the SHG intensity shows a local maximum (resonance). On the other hand, the maximum SHG is recorded at a FW of ≈1500 nm, which corresponds to the 1*s* state of the A exciton (see Figure 1b). We observed the expected quadratic dependence with respect to the fundamental input power for both SHG and TP-PL (Figure 3c,d).

Finally, linear polarization-dependent measurements on the SHG (see Experimental Section) at a FW of 1600 nm show a clear six-fold pattern (Figure 3e), as expected for TMDs given their crystal symmetry (see, *e.g.*, [42,43]). The symmetric intensity between the lobes in the recorded sixfold pattern supports the absence of strain in our sample.[44] On the other hand, the measured polarization dependence of TP-PL for a FW of 1360 nm shows a fully isotropic response (Figure 3f). This suggests that in our experimental conditions, the valley coherence (*i.e.*, a coherent superposition of *K* and *K′* valley states) is lost on a timescale (much) shorter compared to internal recombination (from 2*p* to 1*s* state) and radiative emission from the A exciton. As valley coherence is very sensitive to relaxation processes, this could be due to ultrafast intervalley scattering mediated by phonons.[45,46]

2.2. Nonlinear Detection of VP at Different Wavelengths

Next, we move our attention to the possibility of simultaneously exciting (write) and detecting (read) the VP in our sample.

Generation of the VP is obtained by tuning the ellipticity of the fundamental beam (angle ϵ in Figure 2d), which in turn creates a VP either by excitation of excitons mediated by TPA, and thus a population imbalance ΔN as discussed in reference,[38] or by ultrafast coherent effects such as the optical Stark shift.[23] A more detailed discussion on the mechanism of the excitation of the valley imbalance is provided in the next paragraph (Section 2.3). Here, we focus instead on the detection part. As previously discussed, generation of a VP leads to a measurable shift in the polarization of the emitted SHG in comparison to the intrinsic case. The rotation angle of the polarization can be expressed as[38] (see Section S4, Supporting Information)

$$\Phi = arctan(|\chi^{(2)}_{VP}|/|\chi^{(2)}_{I}|) \quad (1)$$

and thus, by measuring the polarization shift Φ, we can directly estimate the ratio between the absolute values of the valley-induced ($|\chi^{(2)}_{VP}|$) and the intrinsic ($|\chi^{(2)}_{I}|$) nonlinear susceptibilities.

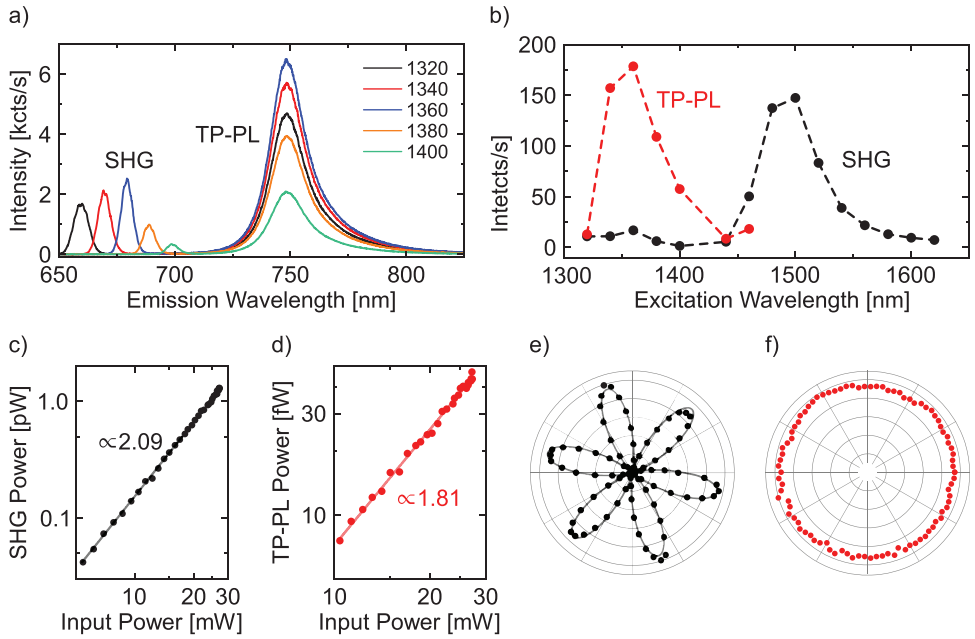

Figure 3. Characterization of SHG and TP-PL in monolayer WSe_2. a) Exemplary spectra of SHG and TP-PL emission at excitation FWs 1320, 1340, 1360, 1380, and 1400 nm. b) Wavelength dependence of the integrated TP-PL (red) and SHG (black). The resonances in the SHG at 1500 nm and in the TP-PL at 1360 nm correspond to the 1*s* and 2*s*/*p* states, respectively. Both SHG c) and TP-PL d) have a quadratic dependence on the excitation power. The measured SHG sixfold pattern, measured at a FW of 1600 nm, e) confirms the absence of strain and reveals the armchair angle, while TP-PL, measured at a FW of 1360 nm, f) results in a fully isotropic emission, pointing toward the absence of valley coherence.

As an example, we report in **Figure 4**a the polarization dependence of the SHG for a FW of 1500 nm, angles ϵ of -25°, 0°, and 25° and input power of 12 mW. After correction (see Section S3, Supporting Information), we observe that the SHG emission at ϵ = 25° rotates anti-clockwise by 9.97° compared to the linear case (ϵ = 0°). When reversing the ellipticity (ϵ = − 25°), the pattern rotates in the opposite direction (clockwise) by 6.38° due to a change in sign of the VP.

In Figure 4b, we plot the SHG rotation angle as a function of the ellipticity of the fundamental beam (angle ϵ) for three different FWs of 1360, 1500, and 1600 nm, corresponding to 2*p* resonant, 1*s* resonant and below gap SHG, respectively. From this, and based on the expression in Equation 1, we can extract a maximum $|\chi^{(2)}_{VP}|/|\chi^{(2)}_{I}|$ of 1.79 %, 18.77 %, and 1.88 % for 1360, 1500, and 1600 nm, respectively: the $|\chi^{(2)}_{VP}|/|\chi^{(2)}_{I}|$ at resonance with the 1*s* (1500 nm) is one order of magnitude larger compared to the cases of resonance with the 2*p* (1360 nm) state and below gap SHG (1600 nm). Considering that the SHG intensity scales with the square of the $\chi^{(2)}$, this corresponds to a valley SHG at least 100 times stronger in the case of 1*s* resonant excitation compared to the other investigated wavelengths. To confirm our results, we performed TDDFT calculations (see Section S5, Supporting Information) for the 1*s* resonant case at 1500 nm (see red open triangles in Figure 4b) and observe excellent qualitative and quantitative agreement. We conclude that, although this approach does not allow for a quantitative estimate of the VP, all-optical resonant detection of the 1*s* exciton state is the most sensitive probe for valleytronic applications. Furthermore, we stress that valley

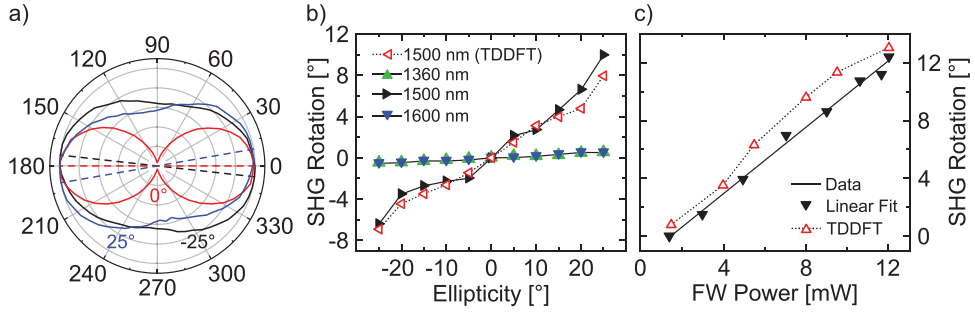

Figure 4. Nonlinear spectroscopy of valley polarization. a) Polarization and tilt angle of the emitted SHG for a FW of 1500 nm and input ellipticities of 0° (red), 25° (blue), and -25° (black). b) Experimentally measured and simulated SHG rotational angle as a function of the input ellipticity. Measurements were carried out for different FW of 1360 nm (green triangles), 1500 nm (black triangles) and 1600 nm (blue triangles). Simulations of the SHG rotation using TDDFT (red empty triangles) for a FW of 1500 nm agree well with the experimental data. c) Experimentally measured (black triangles) and simulated (red empty triangles) SHG rotation angle as a function of the input power for a FW of 1500 nm and ellipticity angle of 30°.

SHG is a versatile method, which can probe (read) the VP regardless of the method that was used for its generation (write)(see Section S6, Supporting Information).

2.3. Coherent Excitation of VP by Below Gap Excitation and Optical Stark Shift

We now discuss in detail the valley SHG from the perspective of the excitation (write) state. In the experiments we simultaneously excite (write) and detect (read) the VP using a single laser pulse, indicating that our results must be a combination of the wavelength-dependent efficiency (dispersion) of the two effects. Since all the investigated FWs are well below the optical gap (≈750 nm) of our sample, we can safely exclude generation of a VP by single photon absorption. Thus, in our conditions, VP can only be generated either by TPA or by a coherent effect (*e.g.*, optical Stark shift). TPA is a $\chi^{(3)}$ process, where two photons are simultaneously absorbed to generate a real population in one of the valleys *via* an intermediate virtual state (Figure 1b). The optical Stark effect, instead, is a process where coherent interaction with off-resonance light leads to a shift in energy levels. Such shift (δ) is inversely proportional to the detuning, $\delta = 2SE_p^2/\hbar\Omega$, where S is the optical Stark shift constant related to the transition dipole moment, E_p is the electric field of the pump laser and $\hbar\Omega$ is the energy difference between the photon energy and the gap.[23] This implies that close to resonance excitation ($\hbar\Omega \to 0$) leads to a larger optical Stark shift. However, several experiments reported a sizable optical Stark shift in TMDs even for large values of the detuning.[23,47,48] In TMDs, the valley selectivity of this process allows introducing a valley imbalance by shifting the energy of the levels in the K' relative to the K valley (Figure 2b).[23,24] Therefore, the generation of a VP by the optical Stark effect does not require the presence of a real exciton population.

Indications that TPA is not playing a major role in our experiments can be already deduced by recalling that: (i) TPA on the 1*s* state is forbidden in the dipole approximation, while it should be maximized for excitation at 1360 nm (2*p* state) (see Figure 1b); (ii) the polarization dependence of the TP-PL at 1360 nm shows no coherence. To further confirm this hypothesis, we performed power-dependent valley SHG at ellipticity of 30° (see Section S5, Supporting Information, for comparison with an ellipticity of 20°), as shown in Figure 4c. In the case of TPA, the VP arises from a real exciton population, which would scale quadratically with the input power.[28] Accordingly, since the valley-induced susceptibility $\chi_{VP}^{(2)}$ is proportional to the VP, also the SHG rotation should scale quadratically with the FW input power. In contrast, the Stark effect shifts the energy levels, and thus the SHG rotation, linearly with respect to the FW pump power.[23] Neither experimental results nor TDDFT simulations indicate a quadratic scaling of the SHG rotation with respect to the input FW power (Figure 4c), while they are well reproduced by a linear fit (black line in Figure 4c). Thus, experiments and simulations both support our assignment of coherent ultrafast generation of the VP *via* optical Stark effect.

3. Conclusion

In conclusion, we studied nonlinear valleytronics in a monolayer WSe_2 sample by investigating the polarization of the SHG as a function of input ellipticity, wavelength and power. First, we showed that the valley SHG is enhanced at resonance with the 1*s* exciton state, where the valley SHG is more than two orders of magnitude stronger compared to above and below gap excitation/detection. Second, we showed that in our experimental conditions the VP is generated *via* a coherent effect that scales linearly with the input power, which we assigned to optical Stark shift. Our results may also explain other recent works performed under similar experimental conditions, where, however, the excitation mechanism of VP was not discussed.[39] Since both SHG and the optical Stark effect are coherent/parametric ultrafast processes, this work points toward the possibility of realizing ultrafast all-optical valleytronic devices, with speed limited only by the duration of the pulses used for the write/read states.

4. Experimental Section

Sample Fabrication and Characterization: WSe_2 monolayer samples were prepared by mechanical exfoliation from a bulk crystal (HQ-Graphene) using an adhesive tape (Nitto) and deposited on a fused silica substrate. Monolayer regions were identified by optical microscopy and confirmed by micro-photoluminescence spectroscopy. The sample was excited using a CW laser (Cobolt 08-DPL 532 nm), which was guided through a 50x objective with a numerical aperture of 0.42 (Mitutoyo Plan Apo), resulting in a focal spot of 1 μm diameter.

Polarization Resolved Multi-Photon Microscopy: As a FW, the tunable output (1320 to 2000 nm with ≈150 fs FWHM) of an Optical Parametric Oscillator (OPO Levante IR, APE) was used, pumped by an *Yb* mode locked laser (FLINT12, Light Conversion) with a repetition rate of 76 MHz and 100 fs pulse duration. Achromatic half (AHWP05M-1600, Thorlabs) and quarter wave plates (#46-562, Edmund Optics) allowed to individually control the tilt θ and ellipticity ϵ angles. Subsequently, the FW was focused on the sample using a 40x reflective objective (LMM40X-P01, Thorlabs), which gives a focal spot-size of ≈3 μm. The emitted SHG was finally filtered by a shortpass (FESH950, Thorlabs) and a suitable bandpass filter (FBH680-10, FBH750-10 or FBH800-10) and the different elements of the SHG nonlinear susceptibility tensor were extracted from the dependence of the SHG intensity with respect to the angle α of a linear polarizer (WP25M-UB, Thorlabs) placed in front of the single channel detector (silicon avalanche photodiode, APD440A, Thorlabs).

Polarization dependence measurements of the SHG were recorded by rotating the polarization axis θ of the input fundamental beam (while keeping a linear polarization, that is, $\epsilon = 0$, see Figure 1d), and co-rotating the analyzer placed in front of the detector (angle α in Figure 1c) in a parallel configuration. The angles α and θ are both defined with respect to the laboratory x-axis (*i.e.*, $\theta = 0$ is P-polarized light in the lab frame).

The polarization dependence of the TP-PL is recorded by keeping the input polarization of the fundamental beam fixed to $\theta = \epsilon = 0$, while the analyzer in detection was rotated by α.

Supporting Information

Supporting Information is available from the Wiley Online Library or from the author.

Acknowledgements

This work was funded by the Deutsche Forschungsgemeinschaft (DFG, German Research Foundation) through the Collaborative Research Center (CRC) 1375 "NOA" projects B5 (G.S.), B2 (I.S.), and A2 (U.P.), and the International Research Training Group (IRTG) 2675 "Meta-ACTIVE", project number 437527638, subproject A4 (G.S. & I.S.).

Open access funding enabled and organized by Projekt DEAL.

Conflict of Interest

The authors declare no conflict of interest.

Data Availability Statement

The data that support the findings of this study are available from the corresponding author upon reasonable request.

Keywords

2D materials, nonlinear optics, second harmonic generation (SHG), Ttransition metal dichalcogenides (TMDs), valleytronics

Received: February 8, 2023
Revised: April 18, 2023
Published online: May 25, 2023

[1] I. L. Markov, *Nature* **2014**, *512*, 147.
[2] S. Klimmer, O. Ghaebi, Z. Gan, A. George, A. Turchanin, G. Cerullo, G. Soavi, *N. Photonics* **2021**, *15*, 837.
[3] Y. Zhang, X. Bai, J. Arias Muñoz, Y. Dai, S. Das, Y. Wang, Z. Sun, *Light: Sci. Appl.* **2022**, *11*, 216.
[4] I. Paradisanos, B. Urbaszek, *Nat. Phys.* **2023**, *19*, 149.
[5] F. Langer, M. Hohenleutner, C. P. Schmid, C. Pöllmann, P. Nagler, T. Korn, C. Schüller, M. Sherwin, U. Huttner, J. T. Steiner, S. W. Koch, M. Kira, R. Huber, *Nature* **2016**, *533*, 225.
[6] T. Boolakee, C. Heide, A. Garzón-Ramírez, H. B. Weber, I. Franco, P. Hommelhoff, *Nature* **2022**, *605*, 251.
[7] J. S. Ponraj, Z.-Q. Xu, S. C. Dhanabalan, H. Mu, Y. Wang, J. Yuan, P. Li, S. Thakur, M. Ashrafi, K. Mccoubrey, Y. Zhang, S. Li, H. Zhang, Q. Bao, *Nanotechnology* **2016**, *27*, 462001.
[8] E. Eobaldt, F. Vitale, M. Zapf, M. Lapteva, T. Hamzayev, Z. Gan, E. Najafidehaghani, C. Neumann, A. George, A. Turchanin, G. Soavi, C. Ronning, *Nanoscale* **2022**, *14*, 6822.
[9] R. W. Boyd, *Nonlinear optics*, Academic Press, Cambridge, **2020**.
[10] O. Dogadov, C. Trovatello, B. Yao, G. Soavi, G. Cerullo, *Laser Photonics Rev.* **2022**, *16*, 2100726.
[11] G. Soavi, G. Wang, H. Rostami, D. G. Purdie, D. De Fazio, T. Ma, B. Luo, J. Wang, A. K. Ott, D. Yoon, S. A. Bourelle, J. E. Muench, G. Ilya, S. Dal Conte, M. Celebrano, A. Tomadin, M. Polini, G. Cerullo, A. C. Ferrari, *Nat. Nanotechnol.* **2018**, *13*, 583.
[12] K.-J. Tielrooij, *Nat. Mater.* **2022**.
[13] Y. Zhang, Y. Wang, Y. Dai, X. Bai, X. Hu, L. Du, H. Hu, X. Yang, D. Li, Q. Dai, T. Hasan, Z. Sun, *Sci. Adv.* **2022**, *8*, eabq8246.
[14] Y. Li, N. An, Z. Lu, Y. Wang, B. Chang, T. Tan, X. Guo, X. Xu, J. He, H. Xia, Z. Wu, Y. Su, Y. Liu, Y. Rao, G. Soavi, B. Yao, *Nat. Commun.* **2022**, *13*, 3138.
[15] J. R. Schaibley, H. Yu, G. Clark, P. Rivera, J. S. Ross, K. L. Seyler, W. Yao, X. Xu, *Nat. Rev. Mater.* **2016**, *1*, 16055.
[16] G. Wang, A. Chernikov, M. M. Glazov, T. F. Heinz, X. Marie, T. Amand, B. Urbaszek, *Rev. Mod. Phys.* **2018**, *90*, 021001.
[17] K. F. Mak, K. He, J. Shan, T. F. Heinz, *Nat. Nanotechnol.* **2012**, *7*, 494.
[18] H. Zeng, J. Dai, W. Yao, D. Xiao, X. Cui, *Nat. Nanotechnol.* **2012**, *7*, 490.
[19] T. Cao, G. Wang, W. Han, H. Ye, C. Zhu, J. Shi, Q. Niu, P. Tan, E. Wang, J. Liu, Baoli Feng, *Nat. Commun.* **2012**, *3*, 887.
[20] J. Lee, K. F. Mak, J. Shan, *Nat. Nanotechnol.* **2016**, *11*, 421.
[21] K. F. Mak, K. L. McGill, J. Park, P. L. McEuen, *Science* **2014**, *344*, 1489.
[22] G. Wang, X. Marie, I. Gerber, T. Amand, D. Lagarde, L. Bouet, M. Vidal, A. Balocchi, B. Urbaszek, *Phys. Rev. Lett.* **2015**, *114*, 097403.
[23] J. Kim, X. Hong, C. Jin, S.-F. Shi, C.-Y. S. Chang, M.-H. Chiu, L.-J. Li, F. Wang, *Science* **2014**, *346*, 1205.
[24] E. J. Sie, C. H. Lui, Y.-H. Lee, L. Fu, J. Kong, N. Gedik, *Science* **2017**, *355*, 1066.
[25] J. Xiao, Z. Ye, Y. Wang, H. Zhu, Y. Wang, X. Zhang, *Light: Science Appl.* **2015**, *4*, e366.
[26] G. D. Mahan, *Phys. Rev.* **1968**, *170*, 825.
[27] K. He, N. Kumar, L. Zhao, Z. Wang, K. F. Mak, H. Zhao, J. Shan, *Phys. Rev. Lett.* **2014**, *113*, 026803.
[28] Z. Ye, T. Cao, K. O'brien, H. Zhu, X. Yin, Y. Wang, S. G. Louie, X. Zhang, *Nature* **2014**, *513*, 214.
[29] G. Wang, I. C. Gerber, L. Bouet, D. Lagarde, A. Balocchi, M. Vidal, T. Amand, X. Marie, B. Urbaszek, *2D Mater.* **2015**, *2*, 045005.
[30] M. M. Glazov, E. L. Ivchenko, G. Wang, T. Amand, X. Marie, B. Urbaszek, B. L. Liu, *Phys. Status Solidi B* **2015**, *252*, 2349.
[31] K. M. McCreary, M. Currie, A. T. Hanbicki, H.-J. Chuang, B. T. Jonker, *ACS Nano* **2017**, *11*, 7988, pMID: 28763189.
[32] G. Kioseoglou, A. Hanbicki, M. Currie, A. Friedman, D. Gunlycke, B. Jonker, *Appl. Phys. Lett.* **2012**, *101*, 221907.
[33] G. Sallen, L. Bouet, X. Marie, G. Wang, C. R. Zhu, W. P. Han, Y. Lu, P. H. Tan, T. Amand, B. L. Liu, B. Urbaszek, *Phys. Rev. B* **2012**, *86*, 081301.
[34] Z. Wang, A. Molina-Sanchez, P. Altmann, D. Sangalli, D. De Fazio, G. Soavi, U. Sassi, F. Bottegoni, F. Ciccacci, M. Finazzi, L. Wirtz, A. C. Ferrari, A. Marini, G. Cerullo, S. Dal Conte, *Nano Lett.* **2018**, *18*, 6882.
[35] F. Hipolito, V. M. Pereira, *2D Mater.* **2017**, *4*, 021027.
[36] J. Cheng, D. Huang, T. Jiang, Y. Shan, Y. Li, S. Wu, W.-T. Liu, *Opt. Lett.* **2019**, *44*, 2141.
[37] T. Wehling, A. Huber, A. Lichtenstein, M. Katsnelson, *Phys. Rev. B* **2015**, *91*, 041404.
[38] Y. W. Ho, H. G. Rosa, I. Verzhbitskiy, M. J. Rodrigues, T. Taniguchi, K. Watanabe, G. Eda, V. M. Pereira, J. C. Viana-Gomes, *ACS Photonics* **2020**, *7*, 925.
[39] L. Mouchliadis, S. Psilodimitrakopoulos, G. M. Maragkakis, I. Demeridou, G. Kourmoulakis, A. Lemonis, G. Kioseoglou, E. Stratakis, *npj 2D Mater. Appl.* **2021**, *5*, 6.
[40] P. K. Nayak, F.-C. Lin, C.-H. Yeh, J.-S. Huang, P.-W. Chiu, *Nanoscale* **2016**, *8*, 6035.
[41] T. Ehmke, A. Knebl, S. Reiss, I. R. Fischinger, T. G. Seiler, O. Stachs, A. Heisterkamp, *AIP Adv.* **2015**, *5*, 084903.
[42] H. G. Rosa, Y. W. Ho, I. Verzhbitskiy, M. J. Rodrigues, T. Taniguchi, K. Watanabe, G. Eda, V. M. Pereira, J. C. Gomes, *Sci. Rep.* **2018**, *8*, 10035.
[43] M. M. Petrić, V. Villafañe, P. Herrmann, A. B. Mhenni, Y. Qin, Y. Sayyad, Y. Shen, S. Tongay, K. Müller, G. Soavi, J. J. Finley, M. Barbone, **2023**.
[44] L. Mennel, M. M. Furchi, S. Wachter, M. Paur, D. K. Polyushkin, T. Mueller, *Nat. Commun.* **2018**, *9*, 516.
[45] B. R. Carvalho, Y. Wang, S. Mignuzzi, D. Roy, M. Terrones, C. Fantini, V. H. Crespi, L. M. Malard, M. A. Pimenta, *Nat. Commun.* **2017**, *8*, 14670.
[46] Z. Lin, Y. Liu, Z. Wang, S. Xu, S. Chen, W. Duan, B. Monserrat, *Phys. Rev. Lett.* **2022**, *129*, 027401.
[47] D. J. Morrow, D. D. Kohler, Y. Zhao, J. M. Scheeler, S. Jin, J. C. Wright, *Phys. Rev. B* **2020**, *102*, 161401.
[48] E. J. Sie, J. W. McIver, Y.-H. Lee, L. Fu, J. Kong, N. Gedik, *Nat. Mater.* **2015**, *14*, 290.